Thermal Denaturing of Bacteriorhodopsin by X-Ray Scattering from Oriented Purple Membranes

J. Müller, C. Münster, and T. Salditt
Center for NanoScience and Sektion Physik der Ludwig-Maximilians-Universität München, D-80539 Munich, Germany

ABSTRACT We present a temperature-dependent x-ray diffraction study of thin films of purple membranes (PMs) with the native membrane protein bacteriorhodopsin (BR). The high degree of alignment with respect to the silicon substrates allows for the application of modern interface-sensitive scattering techniques. Here we focus on the structural changes of BR in PMs at the thermal denaturing transition. A partial unfolding of the helices is observed rather than the complete unfolding process known from helix to coil transitions. While BR remains threaded into the lipid bilayer in the denatured state, changes in the short-range lateral structures are associated with the partial unfolding of the transmembrane helices.

INTRODUCTION

Thermal denaturing of proteins as an often irreversible loss of their biologically active conformational state is an important and well-studied phenomenon. In the case of water-soluble proteins, many different aspects of the unfolding process, including kinetic effects of thermal denaturing (Lumry and Eyring 1954) and fundamental motifs such as the helix-coil transition (Poland and Sheraga 1979), are well understood. In contrast, much less is known about the denaturing of integral membrane proteins, which are critical components in a broad range of biological functions, such as nerve conduction, energy conversion, active ion and molecular transport, and molecular recognition (Lodish et al., 1995). Aside from the biological and biophysical interest in the elucidation of their folding and reverse folding pathways, structural integrity is also required in a growing number of biomaterials and biotechnology applications of BR (Birge, 1990; Hampp, 1992), some of which may include high operating temperatures.

In this work we study the thermal denaturing of the integral membrane protein bacteriorhodopsin (BR) by synchrotron-based x-ray scattering from oriented multilamellar membranes. In its native form, BR is a protein of 248 amino acids and is found in the purple membrane (PM) of the archeon *Halobacterium salinarum*. BR, with its retinal chromophore, works as a light-driven proton pump to provide the energy needed for the cellular metabolism (Oesterhelt and Stoeckenius, 1971). The photosynthesis carried out by the bacterium was elucidated by Blaurock, Oesterhelt, and Stockenius in the early 1970s. Two-dimensional (2D) crystallography using cryoelectron diffraction techniques on single PM patches was used to reveal the strongly hierarchical structure of the BR self-assembly in the purple membrane (Henderson et al., 1990). Accordingly, each BR molecule consists of a polypeptide chain folded into seven transmembrane α-helices (secondary structure), which are threaded into the membrane and connected by disordered loops (Belrhali et al. 1999), partially extending into the aqueous environment, thus forming the tertiary structure. As a quaternary structural motif, three BR molecules associate to a trimer configuration, which in turn forms the unit cell of the hexagonal 2D protein lattice in the native PM (quinternary structure). More recently, the structural changes associated with proton pumping could be determined by x-ray crystallography to better than 2 Å resolution (Luecke et al., 1999). Subnanometer resolution of structural changes in membrane proteins in real space has also been demonstrated by atomic force microscopy studies (Müller et al., 1997).

Previous synchrotron x-ray scattering experiments have revealed an extremely high thermal stability of BR in dry multilayers up to temperatures of 140°C (Shen et al., 1993), owing to strong interbilayer interactions. The strength of the interactions can be tuned by controlling the surrounding vapor pressure, thereby changing the multilayer periodicity d (Koltover et al., 1999). Characteristic of the high thermal stability under dehydrated conditions is the absence of the reversible phase transition from the two-dimensional crystalline phase (2D-c) to the quasiliquid phase (2D-l) at the melting temperature T_m. In the long-known 2D-l phase (Fisher and Oesterhelt, 1979) the quaternary trimer structure rests intact, but the long-range (or quasi-long-range) order of the trimers is melted. However, small changes in the tertiary structure are likely to occur in this phase, as suggested by the well-known reversible shift in the visible absorbance maximum from 560 nm to 460 nm (Brouillette at al., 1987). Recently, the melting transition (2D-c to 2D-l) has been studied quantitatively by x-ray diffraction in view of various physical aspects of two-dimensional melting phenomena (Koltover et al., 1999).

However, to date the denatured state (2D-d) and the denaturing transition of BR are rather poorly characterized

Received for publication 7 December 1999 and in final form 28 February 2000.

Address reprint requests to Dr. Tim Salditt, Center for NanoScience and Sektion Physik der Ludwig-Maximilians-Universität München, Geschwister-Scholl-Platz 1, D-80539 Munich, Germany. Tel.: 49-89-2180-2437; Fax: 49-89-2180-3182; E-mail: salditt@physik.uni-muenchen.de.

0006-3495/00/06/3208/10 $2.00

on the structural level, partly because of the obvious lack of long-range order in this state, while spectroscopic and calorimetric studies have established a number of important results. Accordingly, a shift in the absorption maximum to 370 nm indicates that retinal looses the characteristic protein contacts responsible for the purple color at 560 nm.

In circular dichroism (CD) measurements, relatively small changes in the secondary structure were found upon thermal denaturing, as compared to the changes normally encountered in water-soluble proteins (Brouillette et al., 1987). Likewise, pH denaturing of BR at a fixed temperature is characterized by only ~20% reduction in ellipticity at 222 and 210 nm (Muccio and Cassim, 1979). Furthermore, pH denaturing of BR at 110°C yielded a specific entropy and enthalpy of 3.7 cal/g and 0.01 cal K^{-1}, respectively, indicative of only a partially unfolded state of the denatured protein in the membrane (Brouillette at al., 1987). Infrared absorption measurements have been successfully used to characterize the denaturing pathway of BR (Taneva et al., 1995) and are also compatible with the idea that the intramembranous portions of membrane proteins do not become unfolded upon thermal denaturing (Cladera et al., 1992).

Furthermore, differential scanning calorimetry (DSC) has shed some light on the highly kinetic nature of the irreversible denaturing transition. Accordingly, the folding state at any temperature (within the denaturing range) depends on the time required to reach that temperature (Galisteo and Sanchez-Ruiz, 1993), such that the transition temperature T_d is not properly defined as a thermodynamic quantity. This has been confirmed independently by x-ray diffraction (Koltover, 1998). Therefore, we have selected temperatures in this study where the transition occurred within a time scale of less than an hour, but have kept the sample at high temperatures for up to several days to be able to exclude further unfolding steps. We have carried out an extensive, x-ray scattering study of the denatured state, shedding light on the organization of the denatured protein within the membrane. For this purpose, specular and nonspecular reflectivity and grazing incidence diffraction techniques have been combined with conventional transmission measurements. Most importantly, we present, for the first time, data on the intramolecular scattering peaks of the α-helix around the denaturing transition, yielding insight into the temperature dependence of the helical pitch of BR and the number of helical pitches remaining correlated at high temperatures.

EXPERIMENTAL

Sample preparation

Films were prepared from purified and extensively washed suspensions of PM. The ratio of the optical absorption coefficients at $\lambda = 280$ nm and $\lambda = 568$ nm was 8:5. PM suspended in ultrapure water (Millipore) at (typically) 5 mg/ml was carefully spread onto silicon wafers cut to pieces of ~10 × ~10 mm^2, cleaned by standard procedures, and made hydrophilic by an etch of KOH in ethanol. For x-ray scattering in transmission geometry, ultrathin wafers of a thickness between 20 and 50 μm were used. In this work we prepared only PM patches of native size and did not fuse them to larger entities. Nevertheless, we achieved the same alignment as reported previously (Koltover et al., 1998) for giant fused-patch samples, if the spreaded suspension was allowed to evaporate only very slowly over several days in a closed chamber, and as long as the total film thickness was smaller than ~10 μm. Typically, the thickness of the films was in the range of $D \simeq 1-5$ μm. The high degree of membrane orientation with respect to the substrate of (typically) better than 0.025° was a prerequisite for quantitative specular and nonspecular reflectivity measurements. For the x-ray experiments, the films were kept in a temperature-controlled chamber with a reservoir for water or salt solution. The multilamellar stack could then be swollen from the vapor phase, owing to the repulsive electrostatic forces resulting from an average surface charge density of $\sim 1e^-/(240\ Å^2)$ in PM (Koltover, 1998). By application of a small temperature gradient between sample and reservoir, particularly large multilamellar periodicities d could be obtained.

Specular reflectivity

The samples were then routinely characterized by x-ray reflectivity, e.g., at an in-house rotating anode generator equipped with a bent Ge(110) monochromator selecting CuK_α radiation, a four-circle diffractometer, and a standard NaJ scintillation counter, or for high resolution at synchrotron beamlines (see below). For this method the incident beam with wave vector $\mathbf{k}_i$ has to be collimated to less than a few hundredths of a degree and directed onto the sample at glancing incidence angle α_i. The reflected intensity is then measured as a function of α_i under specular conditions, e.g., at an exit angle $\alpha_f = \alpha_i$, with the wave vector of the exit beam denoted by $\mathbf{k}_f$. Thus the momentum transfer of the elastic scattering $\mathbf{q} = \mathbf{k}_f - \mathbf{k}_i$ is always along q_z, with the z axis parallel to the sample normal (see Fig. 1).

Nonspecular (diffuse) reflectivity

In contrast, changing the detector or sample positions to $\alpha_i \neq \alpha_f$ (diffuse or nonspecular scattering) results in a component $q_\parallel$ parallel to the sample surface. Typically, the reflectivity can be recorded over eight orders of magnitude, after correction for diffuse scattering background, as measured in a so-called offset scan. Beyond background subtraction the diffuse (nonspecular) scattering component contains valuable information on the lateral membrane structure on mesoscopic length scales, particularly the height fluctuations as quantified by the height-height self- and cross-correlations (see, e.g., Holý et al., 1999; Salditt et al., 1994). In Fig. 1 *b* the diffuse Bragg sheets are sketched extending along $q_\parallel$ in the vicinity of the specular Bragg peaks, $q_z = n2\pi/d$.

Grazing incidence diffraction

In grazing incidence diffraction (GID) the x-ray beam impinges at a small angle α_i and is measured at small α_f after being scattered laterally out of the plane of incidence by an angle 2θ (Dosch, 1992; see Fig. 1 *c*). In such a geometry, the reciprocal space can be scanned along $q_\parallel$ at finite q_z (see Fig. 1 *b*), intersecting the rods of the 2D protein lattice.

Helix scattering

The diffraction pattern of the BR α-helices does not rely on intermolecular correlations and can thus be conveniently monitored independently of lateral ordering of the proteins. As an intramolecular interference effect, the signal consists of weak intensity modulations in reciprocal space (see, e.g., Cantor and Schimmel, 1980). Using highly oriented films, the scattering distribution can be mapped in reciprocal space in $q_\parallel$ and q_z, offering

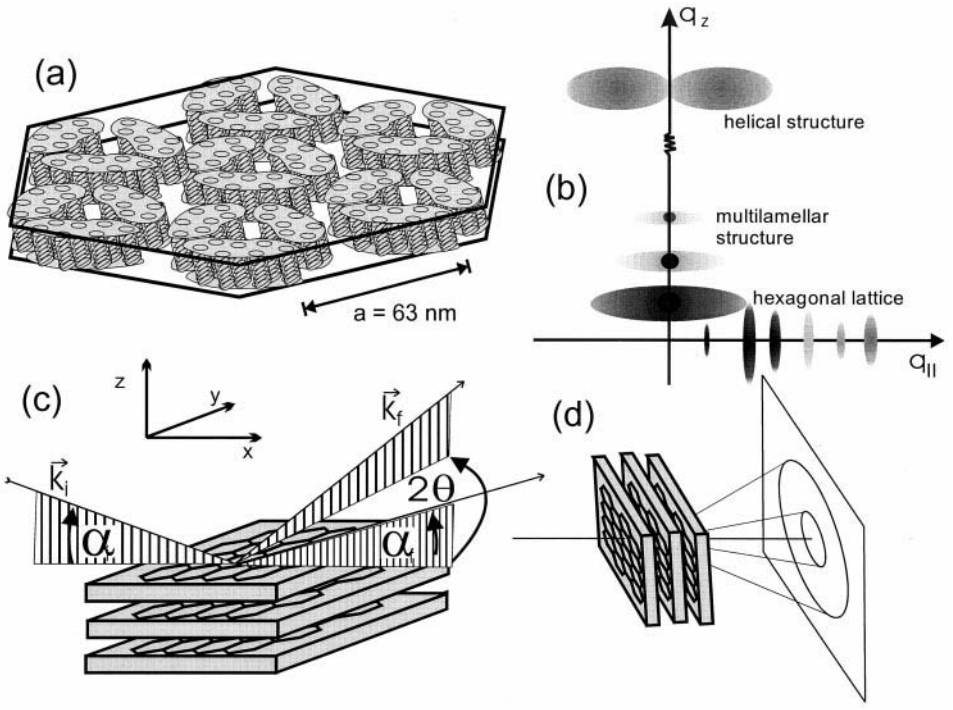

FIGURE 1 (*a*) The hexagonal unit cell of the 2D protein lattice in the PM is sketched with the transmembrane helices of BR. The lipids fill the blank spaces between the protein trimers. (*b*) The corresponding reciprocal space with its characteristic elements, and the schematic of the scattering setup in (*c*) reflection and (*d*) transmission geometry.

a new tool to probe changes in the spatial arrangement of the helices. Here we concentrate on the relatively strong peak originating from the periodicity of the helical pitch, which for BR occurs at 1.28 $Å^{-1}$. The helix scattering in relatively thin (below 5–10 μm) and thus highly oriented films could only be investigated with synchrotron radiation at optimized signal-to-noise ratios. Thicker films, however (typical mosaicities of 1–2°) could also be studied at an in-house rotating anode generator with a focused beam in Bragg-Brentano geometry.

High brilliant synchrotron radiation was particularly important for the measurements of diffuse scattering (e.g., by reciprocal space mappings), GID, and the BR helix scattering from oriented PM, which were all carried out at the bending magnet beamline BM5 at the European Synchrotron Radiation Facility (ESRF), using a *z*-axis diffractometer and a fast scintillation counter (Cyberstar, Oxford Instruments). At a photon energy of 20 keV (set by a double crystal monochromator), no radiation damage was observed, even after several hours of exposure to the beam. Experiments on highly aligned PM films in transmission geometry (see Fig. 1 *d*) were performed at the beamline JUSIFA (HASYLAB/DESY).

RESULTS

As shown recently (Koltover et al., 1998), the high orientational alignment of the multilamellar stack of PMs allows for a quantitative application of interface-sensitive scattering techniques, like specular and nonspecular x-ray reflectivity, diffuse scattering, and truncation rod scattering. In the previous experiments, the alignment was obtained by fusing the small patches of the native bacterial membranes into a 10-μm patch and using these larger crystalline patches to prepare very high-quality multilayers suitable for the application of reflectivity and grazing incidence diffraction techniques. In this work we show that the same highly perfect orientation of PM can be obtained with native, nonfused patches. Typical reflectivity profiles (Fig. 2, *solid symbols*) for such samples are shown for different humidity conditions, i.e., at different multilamellar periodicities *d*. In Fig. 2 *a* the specular reflectivity, along with the corresponding diffuse background (as measured in an offset scan; *open symbols*), is shown for a dry stack in equilibrium with a reservoir of saturated NaCl solution, resulting in a lamellar repeat distance of $d = 50.7$ Å. Pronounced Bragg maxima are modulating the steep decay of the reflectivity curve. The diffuse scattering is also strongly modulated, indicating a conformal corrugation, i.e., a corrugation that is copied across neighboring membranes. The inset shows a typical rocking curve at the first Bragg peak ($\alpha_i + \alpha_f = 0.72°$), with a central width of 0.007° (HWHM), proving the mosaicity to be on the order of the instrumental resolution. It is important to note that the broad diffuse background of the rocking scan does not result from badly oriented or unoriented domains, but from membrane undulation and corrugation, as proved by characteristic refraction effects in reciprocal space.

In Fig. 2 *b* the corresponding curves are shown for a sample that has been swollen to large distances by applying a small gradient in temperature between a salt-free water reservoir and the sample, illustrating the case of vanishing positional correlations in the multilamellar stack. Because of the lack of Bragg peaks the periodicity *d* cannot be determined, because Bragg peaks could typically be resolved only up to $d \simeq 150$−-300 Å. Because in this limit of large *d* the positional correlations vanish, it may also be expected that the interactions between different membranes

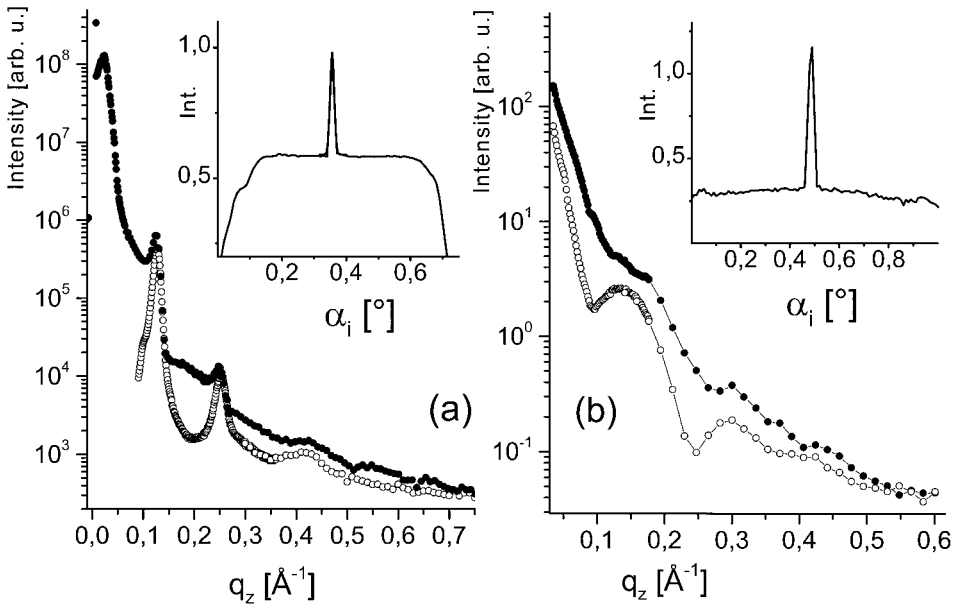

FIGURE 2 Reflectivity and offset scan at (*a*) low and (*b*) high swelling of the PM stack, together with the corresponding rocking scans (*inset*). The high degree of orientational alignment is independent of the swelling condition. At $d = 50.7$ Å in (*a*), strong positional correlations give rise to sharp peaks in the structure factor modulating both the specular and diffuse scattering, while at $d \geq 200$ Å the structure factor becomes unity and the oscillations in the intensity decay reflect solely the form factor of PM.

become negligible. Indeed, the melting temperature T_m of the 2D crystalline phase becomes independent of d in this limit, while the intermembrane forces manifest themselves in a strong d dependence of T_m for smaller separations (Koltover et al., 1999). Because the structure factor describing the vertical correlation of the diffuse scattering is essentially constant, the offset scan is directly proportional to the bilayer form factor averaged in the xy plane.

In Fig. 3, diffraction profiles of PM are shown, as measured in transmission geometry at $T = 30°$, 85°, and 95°C, respectively, on a highly aligned sample of BR spread onto a thin Si wafer. The concentric diffraction pattern on the area detector has been radially averaged and is shown as a function of $q_{\|}$. In the inset, a diffraction profile measured with better counting statistics in the 2D-c phase is shown after background subtraction, yielding a clean diffraction pattern, also at small $q_{\|}$ around the (10) reflection. As is well known, the reflections of the 2D crystalline phase index to

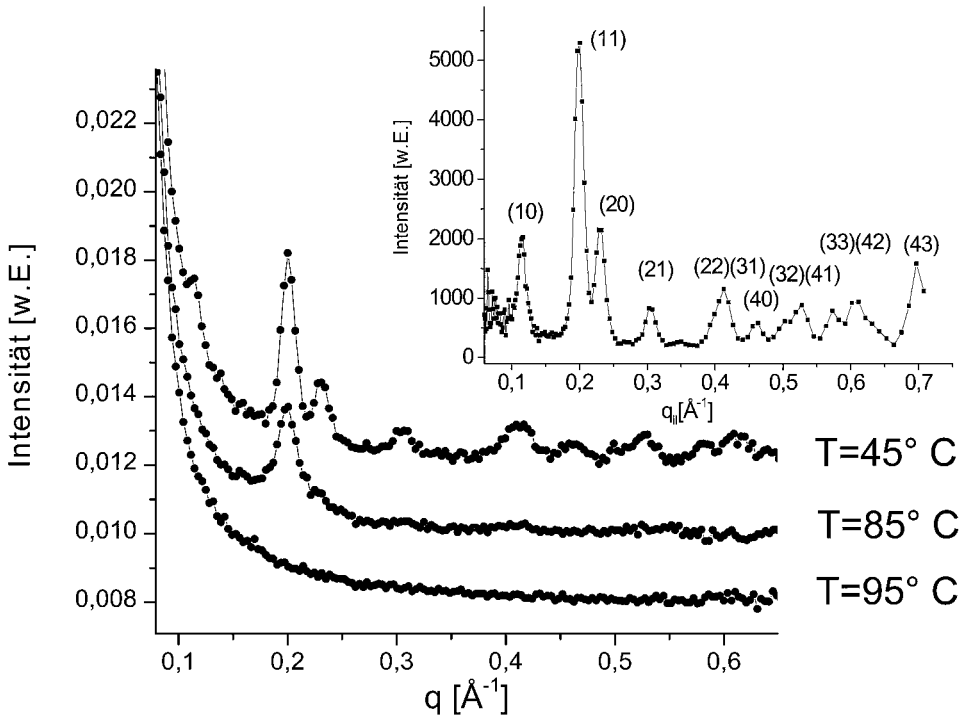

FIGURE 3 The diffraction profiles of PM are shown, as measured in transmission geometry at $T = 30$°C, 85°C, and 95°C, respectively, corresponding to the three distinct phases of BR: two-dimensional solid (2D-c), two-dimensional liquid (2D-l), and the denatured state.

the 2D hexagonal lattice $q_{hkl} = 4\pi/(\sqrt{3}a)\sqrt{h^2 + hk + k^2}$ with a lattice parameter of $a = 63.4$ Å. The width of the hexagonal structure peaks (HWHM = 0.01 $Å^{-1}$) is resolution limited, setting a lower limit to the crystalline domain size of about $L \geq 650$ Å.

As the temperature is raised above the melting transition temperature T_m, the 2D crystalline protein lattice melts to a quasiliquid phase of highly correlated trimers (Koltover et al., 1999), with a strong liquid correlation peak remaining at $q = 0.199$ $Å^{-1}$. The maximum of the structure factor at $q_{\|} = 0.199$ $Å^{-1}$ is characteristic of the liquid-like phase, indicating a near-neighbor distance $a = 63.1$ of the trimers and an exponential decay length of the liquid-like short range order of ~115 Å. Note that a first maximum expected at ~0.1 $Å^{-1}$ is suppressed by a minimum of the trimer form factor, while the observed maximums are enhanced by a corresponding maximum (see below and Fig. 4). Surprisingly, the transition temperature of the reversible, first-order melting was found to depend sensitively on the mean vertical distance d between the BR patches, indicating strong intermembrane interactions that render the melting quasi-two-dimensional rather than purely two-dimensional (Koltover et al., 1999). Generally speaking, the higher-order self-assembly up to the multilamellar structure ("sixtenary structure") is strongly coupled to the stability of the lower-order structural levels, down to the secondary structure. By x-ray diffuse scattering on highly oriented samples, we have found further evidence that a leading contribution to interbilayer interactions is made by the steric restrictions on the membrane corrugation. In particular, we found that the melting transition is associated with a strong decrease in the diffuse scattering (Müller and Salditt, unpublished observations). The diffuse scattering can be associated with conformal membrane corrugation (buckling) typical for the crystalline phase (Koltover, 1998).

At still higher temperatures, BR denaturing is accompanied by a further change in the in-plane diffraction profile. The strong correlation maximum vanishes irreversibly at the denaturing transition (see the intensity distribution obtained at $T = 95$°C in Fig. 4 *c*), indicating that the trimer structure is changed in the denaturing process. However, in contrast to the melting transition, almost no changes in the diffuse scattering are associated with this transition, indicating no major lateral inhomogeneity on lateral length scales greater than the trimer. At the same time, the well-known changes in the optical absorption spectrum after the detachment of the retinal result in a change of color from purple to a pale yellow. Unfortunately, the scattering intensity at small $q_{\|}$ was quite high, because the sample was relatively thin and the chamber background relatively strong in this region. To increase the sensitivity in this q range, additional measurements were carried out on thicker samples and with a setup of collimating slits on the detector side in grazing incidence diffraction geometry at the optics beamline of ESRF (see Fig. 4), where $q_{\|}$ was scanned at constant $q_z = 0.071$ $Å^{-1}$, intersecting the rodlike extensions of the lateral correlation peaks. Representative data sets are shown for the structure factor of the three distinct phases of BR: two-dimensional solid (2D-c), two-dimensional 2D liquid (2D-l), and the denatured state. Interestingly, a new peak emerges at $q_{\|} =$

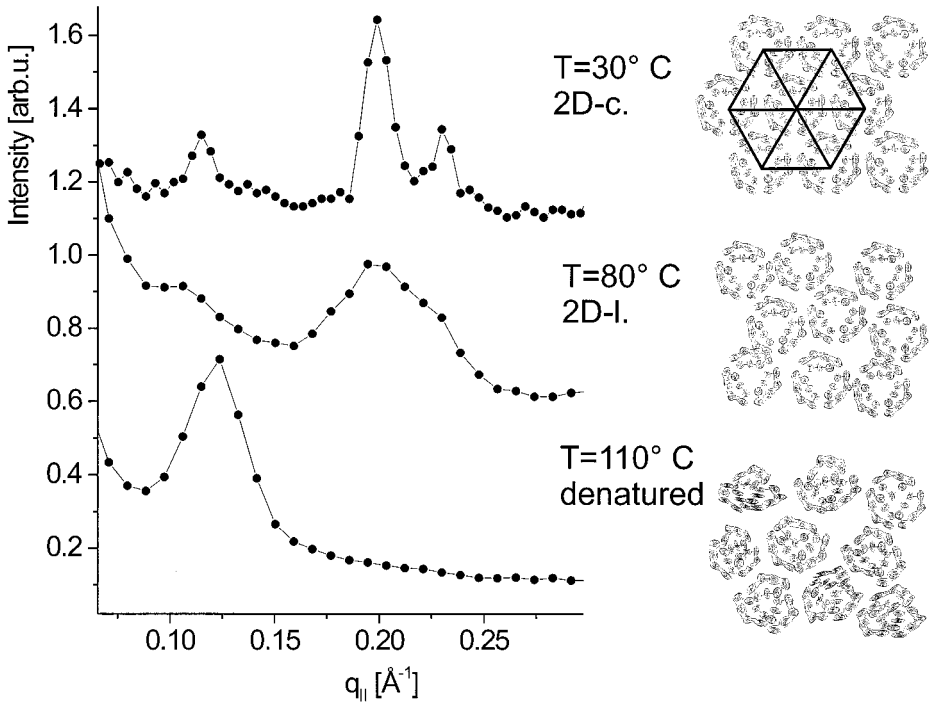

FIGURE 4 The structure factors of the 2D-c, 2D-l, and the denatured state, probed at grazing incidence diffraction, rather than in transmission geometry as in Fig. 3. At a much improved signal-to-background level, a new peak can be observed at ~0.12 $Å^{-1}$ in the denatured state. Possible changes in the trimer structure associated with the denaturing are shown schematically on the right.

0.11 $Å^{-1}$ with rising temperature. Because of the high background level, this peak could not be resolved in the previous transmission setup. The peak is again attributed to liquid-like correlations in the plane of the membrane. The corresponding distance of 57 Å suggests that the correlation is still due to entities of the length scale of a trimer rather a monomer. Indeed, the position of the peak is close to the position where the first liquid-like peak should occur in the 2D-l phase if it was not suppressed by the form factor minimum.

In a simplified model, the form factor can be computed by approximating the electron density projected in the plane of the membrane as an ensemble of point scatterers, each representing a helix. Starting from the coordinates of the 2D-c state, the trimer arrangement can now be distorted by discrete changes in the configuration of the point scatterers. As an illustration, three different configurations are plotted in Fig. 5, along with the corresponding form factors, as obtained after an in-plane powder averaging. Interestingly, the peak emerging in the denatured phase could be easily explained if the roughly ringlike structure of the trimer is distorted to a somewhat more even distribution, with some monomers shifting toward the center. Therefore is plausible to assume that monomers and the trimer are structurally distorted and that the monomers have shifted with respect to each other. Therefore the form factor can be approximated by that of a disk rather than that of a ring.

However, it is quite clear that the secondary and tertiary structures of the monomer must also be strongly affected by the denaturing transition, as discussed below. An important question to be addressed is the extent to which the denatured protein remains in a transmembrane configuration or unfolds into the water region between the lipid bilayers, e.g., with the hydrophobic residues at the inside of some coiled configuration. This would obviously contradict the interpretation given for the peak observed in Fig. 4. More importantly, the specular and nonspecular reflectivity data give evidence that the majority of the BR hydrophobic segments do not unfold out of the lipid matrix, because this would necessarily affect the multilamellar structure of the purple membrane. After all, ~75% of the total mass of PMs is made up of protein.

Let us now turn to the diffraction signal from the BR α-helix. As an intramolecular interference effect it does not rely on intermolecular correlations and can thus be conveniently monitored independently of lateral ordering. At the same time it gives direct evidence for the structural integrity of the α-helices and is expected to change upon denaturing. As has been noticed very early (Henderson, 1974), the helical pitch in BR differs distinctly from the value of 5.4 Å expected for a free helix: the axial reflection occurring at ~1.28 $Å^{-1}$ indicates a pitch of ~4.9 Å. Here we have monitored the peak position, intensity, and width over a wide range of temperature and humidity, covering three distinct structural states of the protein (2D crystal, 2D quasiliquid, and denatured). In Fig. 6, representative data sets at three different temperatures are shown for the helix peak at 1.28 $Å^{-1}$. The sample was in equilibrium with a water bath of saturated NaCl solution. To increase the signal-to-noise ratio, a relatively thick sample with a total thickness of roughly $D = 20$ μm, corresponding to a few thousand layers of PM, was chosen. In this thickness range, mosaicities typically were in the range of 1–2°.

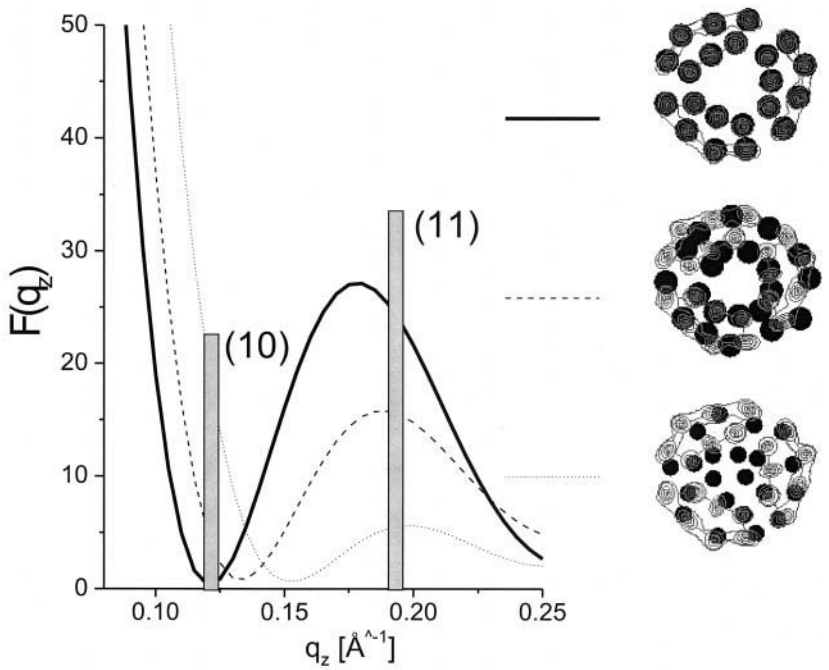

FIGURE 5 The effect of changes in the trimer structure upon the form factor is illustrated in a simplified model (see text). In the 2D-c structure the first minimum of the form factor suppresses the (10) peak and enhances the (20) and (11) peaks. Similarly, the first maximum in the liquid 2D-l phase is suppressed. In the denatured state, the scenario must be inverted to explain the vanishing of the second peak and the emergence of the first. This may happen through a considerable distortion of the trimer arrangement.

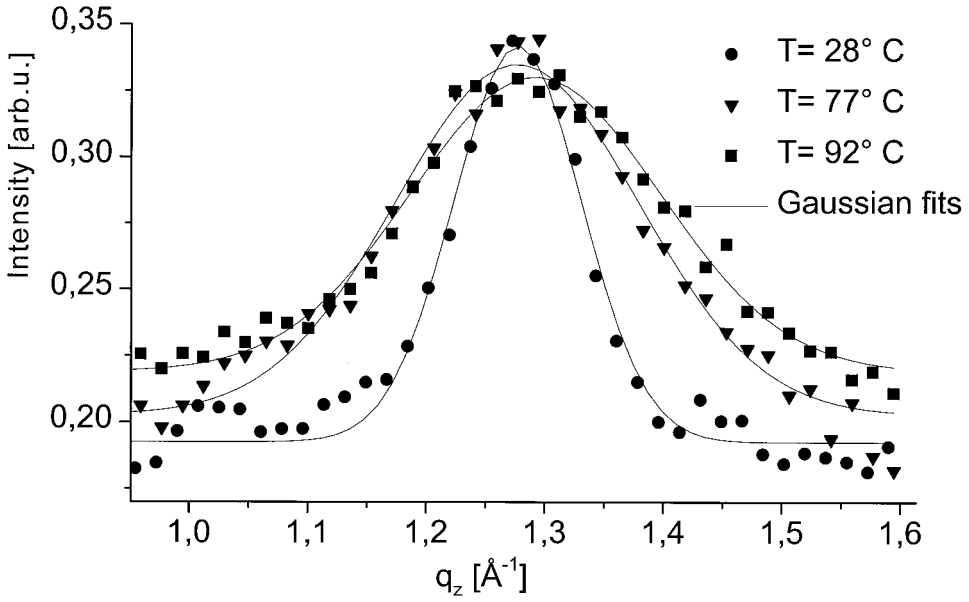

FIGURE 6 The radial profile of the 1.27 $Å^{-1}$ peak corresponding to the helical pitch (helix peak) at different temperatures. The peak is broadened but does not vanish upon denaturing.

Clearly, the peak undergoes distinct and reproducible changes in position, intensity, and, in particular, width, as discussed in detail below. Up to the denaturing transition all changes are completely reversible, as expected. Surprisingly, however, a broadened helix peak remains in the denatured state, indicating considerable helical folding, even in the denatured state. At $T = 92°C$, for example, the sample of Fig. 6 had already denatured, but still showed a pronounced helix peak. The helix peak remained intact over the whole time range probed (up to several days for some samples) and thus is not the result of a slow unfolding kinetics. Moreover, samples were kept at 120°C for several days and still showed the same effect. Thus we can safely conclude that the equilibrium structure at high temperatures is a partially unfolded state. Because crystalline order is lacking in both the melted and denatured states and the signal observed here results only from intramolecular interference, it is difficult to deduce structural information with specificity to the seven different α-helices in the molecule. One approach to solving this problem is to take data on highly aligned films in the two-dimensional q_z-$q_\parallel$ space and to model the superposition of the scattering signal from the seven helices, starting from the low-temperature structural coordinates. While we have not yet completed such a study, we have successfully shown that thinner samples of about $D = 2$ μm can indeed be oriented with respect to a substrate by better than 0.01° and have used such samples to map out the scatting distribution around the helix peak at 1.28 $Å^{-1}$ (see Fig. 8) in radial and angular directions, in contrast to Fig. 7, where the peak profile has been recorded only along the radial direction in q_z. The disadvantage is obviously a reduced signal-to-background ratio, as compared to thicker samples, e.g., the sample of Fig. 6.

In Fig. 7 the two-dimensional scattering distribution is shown comparatively for (*a*) $T = 30°C$ and (*b*) $T = 95°C$. Note the anisotropic scaling in q_x and $q_\parallel$ and the (*white*) segments in the plot, which represent the areas of reciprocal pace that are inaccessible to x-rays because of shading effects of the substrate. In this representation, the helix peak is seen as a broad band at about $q_z = 1.28$ $Å^{-1}$ and remains prominent in the denatured state (Fig. 7 *b*). Note that the band (sheet) of intensity has two off-axis broad maxima in the low-temperature phases (2D crystalline and 2D liquid). With denaturing a weakening and broadening of the band is observed, compatible with what is observed in radial scans (e.g., Fig. 6). However, the loss in scattering signal is most pronounced in the off-axis regions, such that the intensity distribution along $q_\parallel$ becomes flat in the denatured state. The positions of the side (off-axis) peaks that are observed at low temperature are compatible with the form factor of a single helix. However, it has to be kept in mind that the intensity distribution corresponds to a convolution of the scattering signal of tilted and untilted helices in BR, and currently no information specific to the individual helices of the BR bundle is available. However, future experiments on highly aligned films in conjunction with careful modeling could shed some light on this point.

We now address temperature-dependent changes of the radial peak profile in more detail, but coarse-graining over the seven different helices in the BR molecule. The center of the helix peak varied systematically with temperature. At lower temperatures ($T = 30°C$) a value of $q_c = 1.277 \pm 0.005$ $Å^{-1}$ was found, whereas the peak center shifted by almost 0.01 $Å^{-1}$ with heating (see Fig. 8). The general trend of a decrease in peak position and therefore an increase in the helical pitch was observed for all samples. A linear

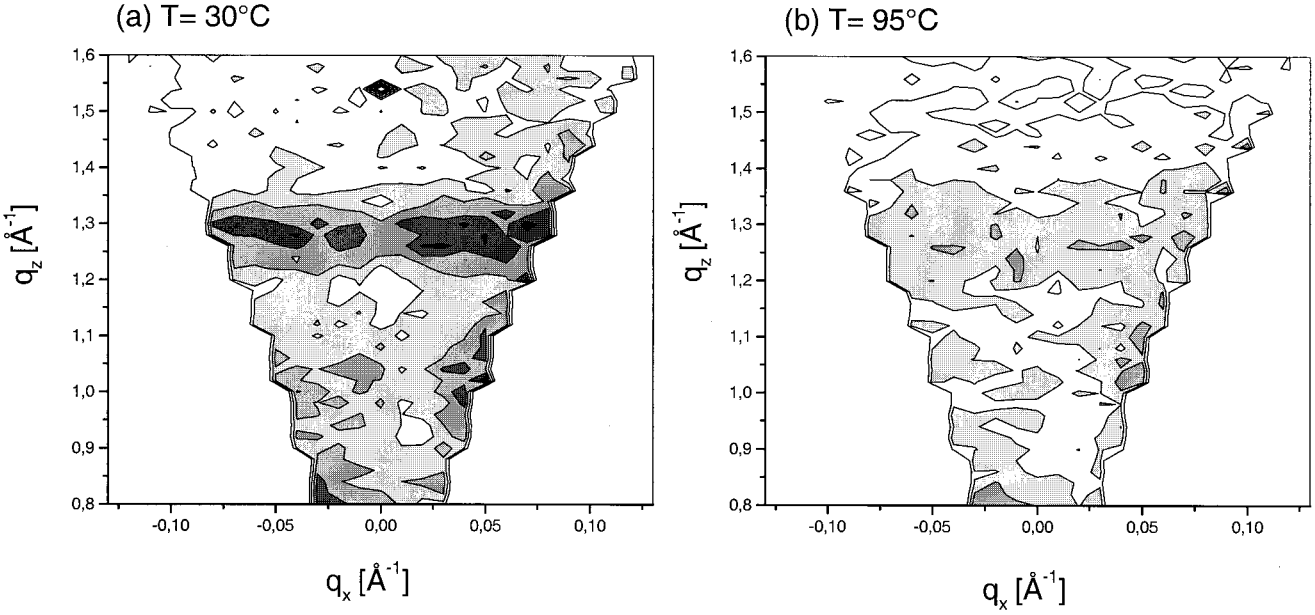

FIGURE 7 Two-dimensional mapping of the reciprocal space around the 1.27 $Å^{-1}$ peak in (*a*) the 2D-c phase and (*b*) the denatured phase.

least-squares fit to the data of Fig. 8 yields a thermal expansion coefficient for the helical pitch of $\alpha_h = (1.1 \pm 0.2) \times 10^{-4}\ K^{-1}$, a result that can be compared to simulations of molecular dynamics (K. Schulten, private communication). Within the experimental errors, the melting transition does not have a noticeable effect on the peak position. A clear discontinuity, however, is observed at the denaturing transition with a pronounced jump to a higher value.

More pronounced than the changes in the center position are the changes in the peak width, shown in Fig. 9, after a combination of several data sets. Despite the spread in the data points resulting from problems in fitting the peak at low peak-to-background ratios, it is quite unambiguous that the width increases significantly at the denaturing transition. However, it does saturate at a finite value, corresponding to a minimum number of helical pitches in registry, $N_{min} \simeq 2$. We can write the width as

$$\mathrm{FWHM} \propto \frac{1}{N_{min} + (N_{max} - N_{min}) f(T)}, \qquad (1)$$

with the average number of helical pitches $N_{max} \simeq 6.5$ in the folded state, and $0 \leq f(T) \leq 1$, the fractional helicity, defined as $(N - N_{min})/(N_{max} - N_{min})$. $f(T)$ can be treated as an order parameter of the unfolding transition. Following

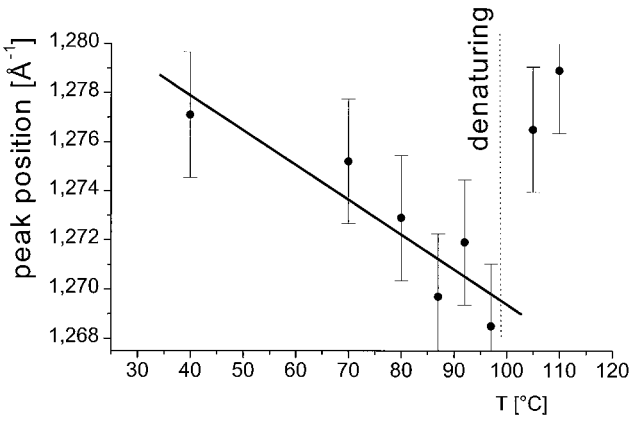

FIGURE 8 The temperature-dependent shift of the center of the helix peak. The thermal expansion coefficient of the helix can be inferred from the data. At the denaturing transition an irreversible jump is observed.

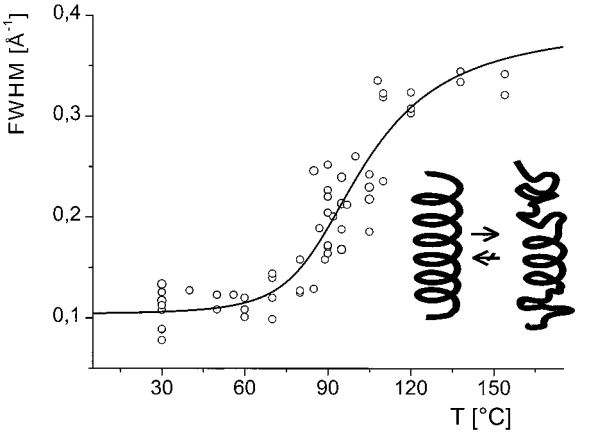

FIGURE 9 The increase of the peak width (FWHM) corresponding to the partial unfolding of the helix. The solid line is a simulation according to the model explained in the text. Importantly, unfolding is never complete and the helical structure is partially preserved in the denatured state.

Zimm and Bragg (1959) in the simple statistical treatment of helix-coil transitions in aqueous proteins, we can express f by

$$f = \frac{s}{1 + s + \sqrt{(1 - s)^2 + 4\omega s}}\left(1 + \frac{s - 1 + 2\omega}{\sqrt{(s - 1)^2 + 4\omega s}}\right). \quad (2)$$

In this model ω is the statistical weight of an event where an isolated helical nucleus is formed, and s is the statistical weight of an event where an additional helical segment (pitch) is folded onto an existing nucleus (see also Cantor and Schimmel, 1980). S can be related to the molar enthalpy difference ΔH_g needed to fold one additional segment,

$$\ln s = \frac{\Delta H_g}{R}\frac{T - T_d}{TT_d}. \quad (3)$$

The solid line in Fig. 9 is a simulation of Eq. 2 with parameters $T_d = 84.3°C$, $\Delta H_g = 890$ J/mol, and $\omega = 10^{-4}$. These values have to be considered with caution because three parameters are strongly correlated. Surprisingly, the simple model is in good agreement with the data and yields reasonable results of the parameters. To our knowledge, this is the first time that the model was applied to the case of a transmembrane protein. However, two important points be kept in mind: 1) Equation 1 was introduced in an ad hoc manner to adapt the model, which was derived for complete and reversible helix-coil transitions. In contrast, the denaturing transition of bR is neither reversible nor complete. 2) The saturation value of the width may not be due to an unfolding of $N_{max} - N_{min}$ turns, but alternatively to a distortion of the complete helix.

DISCUSSION AND SUMMARY

Previous results from calorimetric studies have revealed a dependence of the denaturing enthalpy on the temperature of the transition T_d, which was controlled by the pH. This dependence is believed to result from the exposure of buried hydrophobic groups to the aqueous environment during unfolding (Baldwin, 1986). On the basis of this evidence, it was speculated that the denaturing of BR was accompanied by a disruption of the membrane, resulting in the exposure of membrane-soluble residues to water. This scenario can clearly be excluded from our results, because we observe the conservation of the multilamellar ordering in the reflectivity data. Moreover, it would be hard to reconcile this picture with the finding of oriented α-helical components. Our data, however, would not contradict the generation of new aqueous loops (Brouillette et al., 1987) or increased motion of the transmembrane segments perpendicular to the membrane plane (Dumont et al., 1985), which can both explain the enhanced susceptibility to proteolysis found in denatured BR. Apart from the partially conserved secondary structure, our data indicate a short-range order in the lateral direction with a correlation distance that is only slightly smaller than the nearest-neighbor distance of the trimers. The electron density within such a unit, however, has lost the roughly ringlike trimer structure characteristic of the low-temperature phases and must be more evenly distributed to account for the observed form factor changes. This would be in agreement with calorimetry results, which indicate that denatured BR may be monomeric (Kahn et al., 1992). While BR can be completely renatured in the presence of detergents and free retinal (Huang et al., 1981; London and Khorana, 1982), the transition is irreversible in the native purple membrane, stressing the importance of lipid-protein interaction and structural organization in the membrane. While some aspects of the denatured BR configuration in the membrane could be elucidated in the present work, it is clear that the problem can be completely solved only by a combination of several techniques.

If denaturing is associated with a partial rather than complete vanishing of the secondary structure, the formation of new loops or loop configurations may play an important role. In this picture, it would be easy to understand why steric restrictions between adjacent bilayers may be responsible for the extreme thermal stability in dry films, and why generally the denaturing transition is so strongly dependent on the interbilayer distance. Moreover, a suppression of the melting transition and the shift of the unfolding transition to higher temperatures could possibly be linked to the recent finding that the BR lattices of dehydrated membranes lock positionally in a short-range stacking order (Koltover, 1998). In this sense, the multilamellar arrangement of PM can be regarded as a sixtenary structure of BR, which has important implications for the phase diagram and thermal stability of BR. Experimentally, the interbilayer interactions can be controlled by swelling the multilamellar periodicity d at different vapor pressures. In general, each level of hierarchical order of the BR self-assembly seems to stabilize the respective lower orders. Therefore, structural or spectroscopic studies of the folding or reverse folding processes should aim for a complete in situ assessment of the structure on the various levels. To this end, we have shown that x-ray scattering from highly oriented films can be a useful tool. While the present study was carried out under small and moderate swelling conditions, the thermal denaturing in the limit of infinite d still remains to be explored.

In summary, we have shown that thermal denaturing of BR is associated only with a partial loss of the secondary structure, and that the bulk of the protein remains organized within the membrane, most probably still in a trimer configuration. Upon denaturing, the 1.28 $Å^{-1}$ peak broadens irreversibly. The final width corresponds to only about two positionally correlated helical pitches, indicating strong distortions of the helices. The thermal expansion coefficient of the helix (in the folded state) was found to be $\kappa_h = (1.1 \pm 0.2) \times 10^{-4}$. By the application of interface-sensitive scat-

tering techniques on highly aligned PM, the helical peaks can be mapped in two dimensions. With the aid of corresponding numerical modeling, more details of the partial unfolding process could be revealed in the future, eventually including specific information on individual helices. Ultimately, the modeled molecular structure in such a study must simultaneously explain the two-dimensional high-angle data of the helical interference pattern and the two-dimensional mappings in the low-angle region, reflecting the form factor of the tertiary structure. Finally, such studies could help to reveal the temperature-dependent structure of many other protein-rich membrane systems, which are lacking 3D or 2D crystallinity and therefore are not amenable to x-ray crystallography.

The kind support of D. Oesterhelt and his group at the Max-Planck-Institut für Biochemie, which provided the PM suspensions, is gratefully acknowledged. We thank C. Safinya for introducing us to the beautiful low-dimensional physics and biophysics of purple membranes, and I. Koltover for many helpful discussions and an enjoyable collaboration preceding this work. The help of R. Toucolon at the beamline BM5 of ESRF, and the support of G. Goerigk at the JUSIFA beamline of HASYLAB/DESY are also gratefully acknowledged. We further thank H. Gaub for generous help in setting up the sample preparation laboratory, and J. Peisl for continuous support.

This work has been supported by a grant from the Münchner Universitätsgesellschaft.

REFERENCES

Baldwin, R. L. 1986. Temperature dependence of the hydrophobic interaction in protein folding. *Proc. Natl. Acad. Sci. USA.* 83:8069.

Belrhali, H., P. Nollert, A. Royant, C. Menzel, J. P. Rosenbach, E. M. Landau, and E. Pebay-Peyroula. 1999. Protein, lipid and water organization in bacteriorhodopsin crystals: a molecular view of the purple membrane at 1.9 Å resolution. *Structure Fold Des.* 7:909–917.

Birge, R. R. 1990. Nature of the primary photochemical events in rhodopsin and bacteriorhodopsin. *Biochim Biophys. Acta.* 1016:293–327.

Brouillette, C. G., D. D. Muccio, and T. K. Finney. 1987. pH dependence of bacteriorhodopsin thermal unfolding. *Biochemistry.* 26:7431.

Cantor, C. R., and P. R. Schimmel. 1980. Biophysical Chemistry. Freeman, New York.

Cladera, J., M. L. Galisteo, M. Sabes, P. L. Mateo, and E. Padros. 1992. The role of retinal in the thermal stability of the purple membrane. *Eur. J. Biochem.* 207:581–585.

Dosch, H. 1992. Critical Phenomena at Surfaces and Interfaces. Springer Tracts in Modern Physics, Vol. 126. Springer-Verlag, Berlin and New York.

Dumont, M., J. Trewhella, D. Engleman, and F. Richards. 1985. Stability of transmembrane regions in bacteriorhodopsin studied by progressive proteolysis. *J. Membr. Biol.* 88:233–247.

Fisher, U., and D. Oesterhelt. 1979. Chromophore equilibria in bacteriorhodopsin. *Biophys. J.* 28:211–230.

Galisteo, M. L., and J. M. Sanchez-Ruiz. 1993. Kinetic study into the irreversible thermal denaturing of bacteriorhodopsin. *Eur. Biophys. J.* 22:25–30.

Hampp, N., C. Brauchle, and D. Oesterhelt. 1992. Mutated bacteriorhodopsins—competitive materials for optical information processing. *Mater. Res. Soc. Bull.* 17:56–60.

Henderson, R., J. M. Baldwin, T. A. Ceska, F. Zemlin, E. Beckmann, and K. H. Downing. 1990. Model for the structure of bacteriorhodopsin based on high resolution electron cryo-microscopy. *J. Mol. Biol.* 213: 899–929.

Hiraki, K., T. Hamanaka, T. Mitsui, and Y. Kito. 1981. Phase transitions of the purple membrane and the brown holo-membrane: x-ray diffraction, circular dichroism spectrum and absorption spectrum studies. *Biochim. Biophys. Acta.* 647:18–28.

Holý, V., U. Pietsch, and T. Baumbach. 1999. High-Resolution X-Ray Scattering from Thin Films and Multilayers. Springer Tracts in Modern Physics, Vol. 149. Springer-Verlag, Berlin and New York.

Kahn, T. W., J. M. Sturtevant, and D. M. Engleman. 1992. Thermodynamic measurements of the contributions of helix-connecting loops and of retinal to the stability of bacteriorhodopsin. *Biochemistry.* 31: 8829–8839.

Koltover, I. 1998. Structure and interactions in biomaterials based on membrane-biopolymer self-assembly. Ph.D. thesis. University of California at Santa Barbara.

Koltover, I., J. O. Raedler, T. Salditt, K. J. Rothshild, and C. R. Safinya. 1999. Phase behavior and interactions of the membrane-protein bacteriorhodopsin. *Phys. Rev. Lett.* 82:3184–3187.

Koltover, I., T. Salditt, J.-L. Rigaud, and C. R. Safinya. 1998. Stacked 2D crystalline sheets of the membrane-protein bacteriorhodopsin: a specular and diffuse reflectivity study. *Phys. Rev. Lett.* 81:2494–2497.

Lodish, H., D. Baltimore, and J. Darnell. 1995. Molecular Cell Biology. Scientific American Books, New York.

London, E., and H. G. Khorana. 1982. Denaturing and renaturing of bacteriorhodopsin in detergents and lipid-detergent mixtures. *J. Biol. Chem.* 257:7003.

Luecke, H., B. Schobert, H.-T- Richter, J.-P. Cartailler, and J. K. Lanyi. 1999. Structural changes in bacteriorhodopsin during ion transport at 2 Ångstrom resolution. *Science.* 286:255–260.

Lumry, R., and H. Eyring. 1954. Conformational changes of proteins. *J. Phys. Chem.* 58:110–120.

Muccio, D. D., and J. Y. Cassim. 1979. Interpretations of the effects of pH on the spectra of purple membrane. *J. Mol. Biol.* 135:595.

Müller, D. J., C.-A. Schoenenberger, F. Schabert, and A. Engel. 1997. Structural changes of native membrane proteins monitored at subnanometer resolution with the atomic force microscope. *J. Struct. Biol.* 119: 149–157.

Oesterhelt, D., and W. Stoeckenius. 1971. Rhodopsin-like protein from the purple membrane of *Halobacterium halobium. Nature New Biol.* 233: 149–152.

Poland, D., and H. A. Sheraga. 1970. Theory of Helix-Coil Transitions in Biopolymers. Academic Press, New York.

Shen, Y., C. R. Safinya, K. S. Liang, A. F. Ruppert, and K. J. Rothschild. 1993. Stabilization of the membrane protein bacteriorhodopsin to 140 C in two-dimensional films. *Nature.* 366:48–50.

Singer, S. J. 1990. The structure and insertion of integral proteins in membranes. *Annu. Rev. Cell Biol.* 6:247–296.

Taneva, S. K., J. M. M. Caaveiro, A. Muga, and F. M. Goni. 1995. A pathway for the thermal destabilization of bacteriorhodopsin. *FEBS Lett.* 367:297–300.

Zimm, B. H., and J. K. Bragg. 1959. Theory of the phase transition between helix and random coil in polypeptide chains. *J. Chem. Phys.* 31:526.